Characteristics of exciton-polaritons in ZnO-based hybrid microcavities

Jun-Rong Chen,[1] Tien-Chang Lu,[1,*] Yung-Chi Wu,[1] Shiang-Chi Lin,[1] Wen-Feng Hsieh,[1] Shing-Chung Wang,[1] and Hui Deng[2]

[1]*Department of Photonics, National Chiao Tung University, Hsinchu 30050, Taiwan*
[2]*Department of Physics, University of Michigan, Ann Arbor, Michigan 48109, USA*
[*]*timtclu@mail.nctu.edu.tw*

Abstract: Wide bandgap semiconductors are promising materials for the development of polariton-based optoelectronic devices operating at room temperature (RT). We report the characteristics of ZnO-based microcavities (MCs) in the strong coupling regime at RT with a vacuum Rabi splitting of 72 meV. The impact of scattering states of excitons on polariton dispersion is investigated. Only the lower polariton branches (LPBs) can be clearly observed in ZnO MCs since the large vacuum Rabi splitting pushes the upper polariton branches (UPBs) into the scattering absorption states in the ZnO bulk active region. In addition, we systematically investigate the polariton relaxation bottleneck in bulk ZnO-based MCs. Angle-resolved photoluminescence measurements are performed from 100 to 300 K for different cavity-exciton detunings. A clear polariton relaxation bottleneck is observed at low temperature and large negative cavity detuning conditions. The bottleneck is suppressed with increasing temperature and decreasing detuning, due to more efficient phonon-assisted relaxation and a longer radiative lifetime of the polaritons.

OCIS codes: (140.3945) Microcavities; (140.3948) Microcavity devices.

References and links

1. K. J. Vahala, "Optical microcavities," Nature **424**(6950), 839–846 (2003).
2. H. Deng, G. Weihs, C. Santori, J. Bloch, and Y. Yamamoto, "Condensation of semiconductor microcavity exciton polaritons," Science **298**(5591), 199–202 (2002).
3. C. Weisbuch, M. Nishioka, A. Ishikawa, and Y. Arakawa, "Observation of the coupled exciton-photon mode splitting in a semiconductor quantum microcavity," Phys. Rev. Lett. **69**(23), 3314–3317 (1992).
4. J. Kasprzak, M. Richard, S. Kundermann, A. Baas, P. Jeambrun, J. M. J. Keeling, F. M. Marchetti, M. H. Szymańska, R. André, J. L. Staehli, V. Savona, P. B. Littlewood, B. Deveaud, and S. Dang, "Bose-Einstein condensation of exciton polaritons," Nature **443**(7110), 409–414 (2006).
5. A. Amo, D. Sanvitto, F. P. Laussy, D. Ballarini, E. del Valle, M. D. Martin, A. Lemaître, J. Bloch, D. N. Krizhanovskii, M. S. Skolnick, C. Tejedor, and L. Viña, "Collective fluid dynamics of a polariton condensate in a semiconductor microcavity," Nature **457**(7227), 291–295 (2009).
6. G. Christmann, R. Butté, E. Feltin, J.-F. Carlin, and N. Grandjean, "Room temperature polariton lasing in a GaN/AlGaN multiple quantum well microcavity," Appl. Phys. Lett. **93**(5), 051102 (2008).
7. S. I. Tsintzos, N. T. Pelekanos, G. Konstantinidis, Z. Hatzopoulos, and P. G. Savvidis, "A GaAs polariton light-emitting diode operating near room temperature," Nature **453**(7193), 372–375 (2008).
8. M. Saba, C. Ciuti, J. Bloch, V. Thierry-Mieg, R. André, S. Dang, S. Kundermann, A. Mura, G. Bongiovanni, J. L. Staehli, and B. Deveaud, "High-temperature ultrafast polariton parametric amplification in semiconductor microcavities," Nature **414**(6865), 731–735 (2001).
9. I. R. Sellers, F. Semond, M. Leroux, J. Massies, M. Zamfirescu, F. Stokker-Cheregi, M. Gurioli, A. Vinattieri, M. Colocci, A. Tahraoui, and A. A. Khalifa, "Polariton emission and reflectivity in GaN microcavities as a function of angle and temperature," Phys. Rev. B **74**(19), 193308 (2006).
10. E. Feltin, G. Christmann, R. Butté, J.-F. Carlin, M. Mosca, and N. Grandjean, "Room temperature polariton luminescence from a GaN/AlGaN quantum well microcavity," Appl. Phys. Lett. **89**(7), 071107 (2006).
11. J.-R. Chen, T.-C. Lu, Y.-C. Wu, S.-C. Lin, W.-R. Liu, W.-F. Hsieh, C.-C. Kuo, and C.-C. Lee, "Large vacuum Rabi splitting in ZnO-based hybrid microcavities observed at room temperature," Appl. Phys. Lett. **94**(6), 061103 (2009).

#138784 - $15.00 USD Received 29 Nov 2010; revised 3 Jan 2011; accepted 30 Jan 2011; published 16 Feb 2011

12. D. G. Lidzey, D. D. C. Bradley, T. Virgili, A. Armitage, M. S. Skolnick, and S. Walker, "Room Temperature Polariton Emission from Strongly Coupled Organic Semiconductor Microcavities," Phys. Rev. Lett. **82**(16), 3316–3319 (1999).
13. S. Christopoulos, G. B. H. Von Högersthal, A. J. D. Grundy, P. G. Lagoudakis, A. V. Kavokin, J. J. Baumberg, G. Christmann, R. Butté, E. Feltin, J.-F. Carlin, and N. Grandjean, "Room-temperature polariton lasing in semiconductor microcavities," Phys. Rev. Lett. **98**(12), 126405 (2007).
14. R. Butté, G. Christmann, E. Feltin, J.-F. Carlin, M. Mosca, M. Ilegems, and N. Grandjean, "Room-temperature polariton luminescence from a bulk GaN microcavity," Phys. Rev. B **73**(3), 033315 (2006).
15. F. Stokker-Cheregi, A. Vinattieri, F. Semond, M. Leroux, I. R. Sellers, J. Massies, D. Solnyshkov, G. Malpuech, M. Colocci, and M. Gurioli, "Polariton relaxation bottleneck and its thermal suppression in bulk GaN microcavities," Appl. Phys. Lett. **92**(4), 042119 (2008).
16. A. Teke, Ü. Özgür, S. Doğan, X. Gu, H. Morkoç, B. Nemeth, J. Nause, and H. O. Everitt, "Excitonic fine structure and recombination dynamics in single-crystalline ZnO," Phys. Rev. B **70**(19), 195207 (2004).
17. M. Zamfirescu, A. Kavokin, B. Gil, G. Malpuech, and M. Kaliteevski, "ZnO as a material mostly adapted for the realization of room-temperature polariton lasers," Phys. Rev. B **65**(16), 161205 (2002).
18. R. Johne, D. D. Solnyshkov, and G. Malpuech, "Theory of exciton-polariton lasing at room temperature in ZnO microcavities," Appl. Phys. Lett. **93**(21), 211105 (2008).
19. R. Shimada, J. Xie, V. Avrutin, Ü. Özgür, and H. Morkoç, "Cavity polaritons in ZnO-based hybrid microcavities," Appl. Phys. Lett. **92**(1), 011127 (2008).
20. F. Médard, J. Zúñiga-Perez, P. Disseix, M. Mihailovic, J. Leymarie, A. Vasson, F. Semond, E. Frayssinet, J. C. Moreno, M. Leroux, S. Faure, and T. Guillet, "Experimental observation of strong light-matter coupling in ZnO microcavities: Influence of large excitonic absorption," Phys. Rev. B **79**(12), 125302 (2009).
21. S. Faure, C. Brimont, T. Guillet, T. Bretagnon, B. Gil, F. Médard, D. Lagarde, P. Disseix, J. Leymarie, J. Zúñiga-Pérez, M. Leroux, E. Frayssinet, J. C. Moreno, F. Semond, and S. Bouchoule, "Relaxation and emission of Bragg-mode and cavity-mode polaritons in a ZnO microcavity at room temperature," Appl. Phys. Lett. **95**(12), 121102 (2009).
22. R. Schmidt-Grund, B. Rheinländer, C. Czekalla, G. Benndorf, H. Hochmuth, M. Lorenz, and M. Grundmann, "Exciton–polariton formation at room temperature in a planar ZnO resonator structure," Appl. Phys. B **93**(2-3), 331–337 (2008).
23. C. Sturm, H. Hilmer, R. Schmidt-Grund, and M. Grundmann, "Observation of strong exciton–photon coupling at temperatures up to 410 K," N. J. Phys. **11**(7), 073044 (2009).
24. S. Faure, T. Guillet, P. Lefebvre, T. Bretagnon, and B. Gil, "Comparison of strong coupling regimes in bulk GaAs, GaN, and ZnO semiconductor microcavities," Phys. Rev. B **78**(23), 235323 (2008).
25. J.-R. Chen, S.-C. Ling, C.-T. Hung, T.-S. Ko, T.-C. Lu, H.-C. Kuo, and S.-C. Wang, "High-reflectivity ultraviolet AlN/AlGaN distributed Bragg reflectors grown by metalorganic chemical vapor deposition," J. Cryst. Growth **310**(23), 4871–4875 (2008).
26. A. Tsukazaki, A. Ohtomo, T. Onuma, M. Ohtani, T. Makino, M. Sumiya, K. Ohtani, S. F. Chichibu, S. Fuke, Y. Segawa, H. Ohno, H. Koinuma, and M. Kawasaki, "Repeated temperature modulation epitaxy for p-type doping and light-emitting diode based on ZnO," Nat. Mater. **4**(1), 42–46 (2005).
27. R. E. Sherriff, D. C. Reynolds, D. C. Look, B. Jogai, J. E. Hoelscher, T. C. Collins, G. Cantwell, and W. C. Harsch, "Photoluminescence measurements from the two polar faces of ZnO," J. Appl. Phys. **88**(6), 3454 (2000).
28. S. W. Jung, W. I. Park, H. D. Cheong, G. C. Yi, H. M. Jang, S. Hong, and T. Joo, "Time-resolved and time-integrated photoluminescence in ZnO epilayers grown on Al2O3(0001) by metalorganic vapor phase," Appl. Phys. Lett. **80**(11), 1924–1926 (2002).
29. K. Vanheusden, C. H. Seager, W. L. Warren, D. R. Tallant, and J. A. Voigt, "Correlation between photoluminescence and oxygen vacancies in ZnO phosphors," Appl. Phys. Lett. **68**(3), 403–405 (1996).
30. Y. Chen, D. M. Bagnall, H. Koh, K. Park, K. Hiraga, Z. Zhu, and T. Yao, "Plasma assisted molecular beam epitaxy of ZnO on c-plane sapphire: Growth and characterization," J. Appl. Phys. **84**(7), 3912–3918 (1998).
31. E. S. Shim, H. S. Kang, J. S. Kang, J. H. Kim, and S. Y. Lee, "Effect of the variation of film thickness on the structural and optical properties of ZnO thin films deposited on sapphire substrate using PLD," Appl. Surf. Sci. **186**(1-4), 474–476 (2002).
32. N. Antoine-Vincent, F. Natali, D. Byrne, A. Vasson, P. Disseix, J. Leymarie, M. Leroux, F. Semond, and J. Massies, "Observation of Rabi splitting in a bulk GaN microcavity grown on silicon," Phys. Rev. B **68**(15), 153313 (2003).
33. M. Mihailovic, A. L. Henneghien, S. Faure, P. Disseix, J. Leymarie, A. Vasson, D. A. Buell, F. Semond, C. Morhain, and J. Zúñiga Pérez, "Optical and excitonic properties of ZnO films," Opt. Mater. **31**(3), 532–536 (2009).
34. S. F. Chichibu, T. Sota, G. Cantwell, D. B. Eason, and C. W. Litton, "Polarized photoreflectance spectra of excitonic polaritons in a ZnO single crystal," J. Appl. Phys. **93**(1), 756–758 (2003).
35. S. L. Chuang, *Physics of Optoelectronic Devices*, 1st ed. (Wiley, 1995)
36. G. E. Jellison, and L. A. Boatner, "Optical functions of uniaxial ZnO determined by generalized ellipsometry," Phys. Rev. B **58**(7), 3586–3589 (1998).

#138784 - $15.00 USD Received 29 Nov 2010; revised 3 Jan 2011; accepted 30 Jan 2011; published 16 Feb 2011

1. Introduction

Semiconductor microcavities (MCs) have been intensely investigated recently as a solid-state cavity quantum electrodynamics system [1, 2]. When the exciton-photon coupling rate in a semiconductor MC is larger than the decay rates of excitons and photons, new half-matter half-light quasi-particles are formed and generally termed as MC exciton-polaritons (or MC polaritons). Microcavity polaritons are boson like at low densities, and have extremely light in-plane effective mass. These unique MC exciton-polariton properties are very important for the study of the fundamental physical phenomena including strong light-matter interaction [3], solid-state cavity quantum electrodynamics [1], and dynamical Bose-Einstein condensates [4, 5]. Furthermore, the polariton-related optoelectronic devices such as polariton lasers [6], polariton light-emitting diodes [7], and polariton parametric amplifiers have been demonstrated in recent years [8]. The first experimental observation of the strong coupling regime in a MC was reported in a GaAs-based system [3]. Because of the nearly lattice-matched AlGaAs/AlGaAs distributed Bragg reflectors (DBRs) and the high-quality GaAs/AlGaAs quantum wells, the growth and fabrication of GaAs-based MCs with high quality factor (Q) are relatively easy. However, polaritons in GaAs MCs can only survive at cryogenic temperatures due to the low exciton binding energy (effective Rydberg, R_y) of about 10 meV. In contrast, wide-bandgap semiconductor materials have attracted much attention due to their large exciton binding energies and thus the potential to operate at room temperature (RT) [9]. Strong coupling at RT has been reported in MCs containing GaN, ZnO and organic excitons [10–12]. RT polariton lasing in bulk GaN MCs has also been reported [13]. Moreover, polariton dynamics in similar GaN-based MCs were investigated, where a relaxation bottleneck was observed at RT and the relevant mechanisms have been discussed [14, 15]. There are few literatures reporting the dynamic relaxation bottleneck in wide-bandgap MCs as compared with GaAs-based structures.

An alternative wide-bandgap material is ZnO. Its oscillator strength and exciton binding energy (~60 meV in the bulk layer) are even larger than those of nitride-based materials [16], and theoretical analysis has predicted that a bulk ZnO MC is a potentially excellent candidate for the realization of robust polariton-based optoelectronic devices operating at RT and above [17, 18]. Consequently, significant research effort has been devoted to the experimental study of strong coupling in ZnO MCs [11, 19–23]. Of critical importance to the design and operation of polariton devices is the understanding of the polariton dispersion curves and the kinetics of exciton-polaritons in ZnO-based MCs. Nevertheless, in wide-bandgap materials the full anticrossing dispersion curves may not be well-defined since the Rabi splitting energy can be of the same order of magnitude as or much greater than the exciton binding energy [24]. Furthermore, there has been only one report on the exciton-polariton bottleneck effect of the Bragg-mode polariton branch [15], and no study on the dynamics of cavity-mode polaritons has been available in the ZnO MC system. In this study, we report the experimental observation of strong coupling regime in bulk ZnO-based hybrid MCs. Theoretical and experimental study of the effects of exciton scattering states on polariton dispersions are discussed at RT. Furthermore, a systematic study of the polariton population distribution of ZnO-MC over a wide range of temperatures and exciton-photon detuning values (δ) is presented. The relevant mechanisms leading to the possible presence of a polariton bottleneck in ZnO MCs are discussed.

2. Sample structure and experimental details

The device used in this study is a hybrid MC structure consisting of a bulk ZnO 3λ/2 thick cavity sandwiched between a bottom epitaxially grown 30-pair AlN/$Al_{0.23}Ga_{0.77}N$ DBR and a top 9-pair dielectric SiO_2/HfO_2 DBR. The AlN/AlGaN DBR was grown by metalorganic chemical vapor deposition on a 3.25 μm thick GaN buffer layer on *c*-plane sapphire substrate. During the growth, trimethylgallium (TMGa) and trimethylaluminum (TMAl) were used as

#138784 - $15.00 USD Received 29 Nov 2010; revised 3 Jan 2011; accepted 30 Jan 2011; published 16 Feb 2011

group III source materials and ammonia (NH_3) as the group V source material. After thermal cleaning of the substrate in hydrogen ambient for 5 min at 1100 °C, a 30-nm-thick GaN nucleation layer was grown at 520 °C. The growth temperature was raised up to 1040 °C for the growth bulk GaN layer. Then, the 30-pair $AlN/Al_{0.23}Ga_{0.77}N$ (about 2.38 μm) was grown under a fixed chamber pressure of 100 Torr [25]. The bulk ZnO 3λ/2 thick (about 250 nm) cavity was grown on AlN/AlGaN DBR by pulsed-laser deposition system, which is commonly adopted for the growth of ZnO epi-films [26]. The beam of a KrF excimer laser (λ = 248 nm) was focused to produce an energy density ~5–7 $J \cdot cm^{-2}$ at a repetition rate 10 Hz on a commercial hot-pressed stoichiometric ZnO (99.999% purity) target. The ZnO films were deposited with a growth rate ~0.5475 Å s^{-1} at substrate temperature of 600 °C and a working pressure ~9.8×10^{-8} Torr without oxygen gas flow. Finally, the 9-pair SiO_2/HfO_2 (about 1.06 μm) dielectric DBR was deposited by dual electron-beam gun evaporation system to complete the MC structure. The peak reflectivity of the bottom AlN/AlGaN DBR and the top SiO_2/HfO_2 DBR were measured to be about 93% and 97%, respectively, by using the *n*&*k* analyzer system. The schematic sketch of the ZnO hybrid MC is shown in Fig. 1(a). Figures 1(b) and 1(c) show the low- and high-magnification cross-section scanning electron microscopy (SEM) images, respectively. The interfaces between each layer are well defined. The sample surface is smooth without any cracks observed. Furthermore, there is a continuous variation of the layer thickness across the sample, which in turn is used for the study of different exciton-photon detunings.

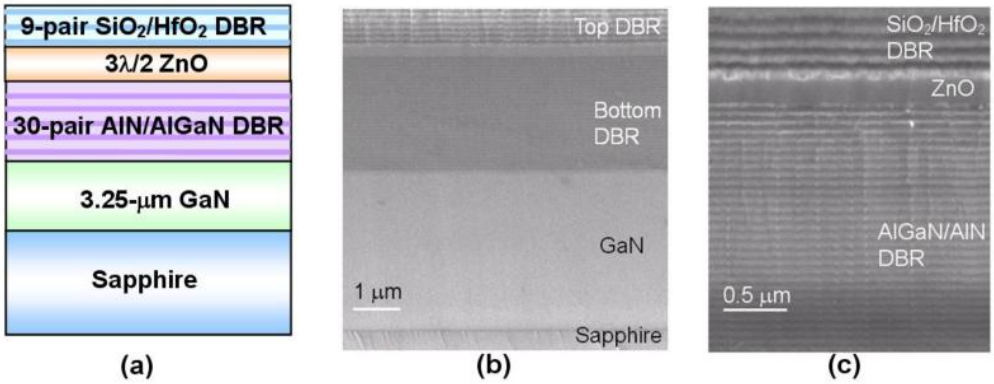

Fig. 1. (a) Schematic sketch of the ZnO MC structure. (b) Low-magnification cross-section SEM image of the 3λ/2 bulk ZnO hybrid MC structure. (c) Cross-section SEM image of the AlGaN/AlN and SiO_2/HfO_2 DBRs, and the 3λ/2 ZnO bulk layer under high magnification.

To probe the polariton dispersion curve, angle-resolved reflectivity measurements were carried out by using a two arm goniometer and a xenon lamp was employed as a white light source fed through a 100 μm core optical fiber. The reflected light was then collected by a 600 μm core UV optical fiber mounted on a rotating stage with an angular resolution of ~1° and detected by a liquid nitrogen cooled charge-coupled device attached to a 320 mm single monochromator with a spectral resolution of about 0.2 nm. As for the observation of exciton-polariton population distribution, off-resonant excitation with a normal incident angle on the sample was performed using a 266 nm radiation of the fourth harmonics of a Nd:YAG pulse laser with a repetition rate of 50 kHz and a pulse duration of 5 ns. The laser spot size on the sample surface was about 120 μm in diameter and the average incident power density was about 50 W/cm^2. The photoluminescence (PL) emission light from the sample surface was collected using a 600 μm UV optical fiber mounted on a rotating stage with an angular resolution of ~1° and also detected by a cooled charge-coupled device attached to a 320 mm single monochromator.

#138784 - $15.00 USD Received 29 Nov 2010; revised 3 Jan 2011; accepted 30 Jan 2011; published 16 Feb 2011

3. Results and discussion

The optical properties of the 3λ/2 ZnO film grown on the 30-pair AlN/AlGaN DBR were investigated by performing RT PL measurements, as shown in Fig. 2(a). The half-cavity structure exhibited strong near-band-edge emission around 378 nm (3.28 eV) [27, 28]. Additionally, the green PL band mainly comes from the deep-level emission which is related to the crystal defects, such as oxygen vacancies and zinc interstitials in the film [29]. The good material quality of the ZnO film can be observed from the suppression of the deep level emission band in the RT PL spectrum [19]. Another feature of the PL spectrum is the long tail extending from the near-band-edge emission. This property is usually observed from RT PL spectra of ZnO films [30], and is caused by band structure deformation due to the crystal lattice deformation. Moreover, it is noteworthy that the increased thickness of a 3λ/2 active layer, with respect to that of a λ/2 or λ cavity, is expected to improve the crystal quality and the optical properties of the ZnO active layer [31].

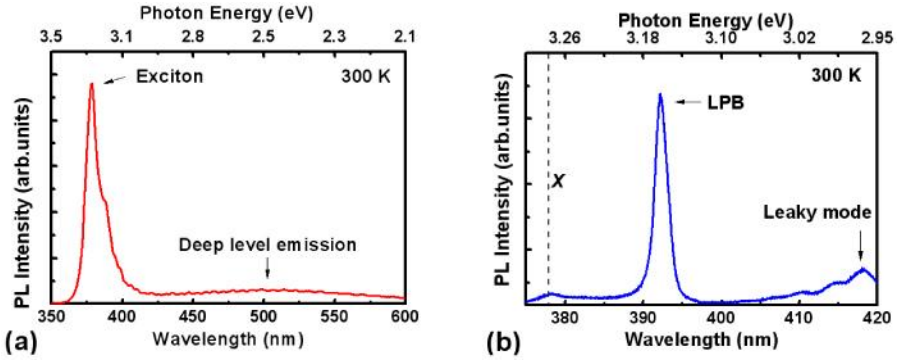

Fig. 2. (a) An RT PL spectrum of the ZnO film grown on 30-pair AlN/AlGaN DBR. The half-cavity structure exhibited strong near-band-edge emission around 378 nm (3.28 eV). (b) An RT normal incidence PL spectrum of the full ZnO hybrid MC structure.

Figure 2(b) shows an RT PL measurement of the full ZnO MC at normal incidence. The vertical dashed line shows the exciton energy and the emission peak energy of the full ZnO MC is about 3.161 eV (λ ~ 392.3 nm), which means that the emission peak is nearly a pure cavity photon mode because of the large negative detuning between cavity photon energy at zero in-plane wave vector and exciton energy. Under this circumstance, we can estimate the intrinsic cavity quality factor with the minimum perturbation of the exciton-photon coupling. From Fig. 2(b), the PL linewidth is about 15 meV (Δλ ~ 1.8 nm) due to the MC effect, and the corresponding cavity quality factor Q (=λ/Δλ) is about 218. The relatively lower Q value compared to that expected from the peak reflectivity of both DBRs may originate from the spatial inhomogeneous broadening of the cavity modes when the collection diameter of the PL emission is as large as 120 μm. Moreover, another relatively weak PL emission peak was observed at 418 nm. This emission originates from the Bragg leaky modes of the top SiO_2/HfO_2 DBR structure.

3.1 Effects of exciton scattering states on polariton dispersions

To further probe the characteristics of strong exciton-photon coupling in the ZnO microcavity structure, RT angle-resolved reflectivity measurements were performed for the observation of in-plane exciton-polariton dispersion curves. The color map of the angular dispersion of measured reflectivity spectra from 8 to 38° is shown in Fig. 3(a). Furthermore, the color map of the calculated angle-resolved reflectivity spectra with taking into account the resonant exciton is shown in Fig. 3(b). In our simulation, the reflectivity spectra were carried out based on the transfer matrix method assuming TE polarization and the resonant exciton was

#138784 - $15.00 USD Received 29 Nov 2010; revised 3 Jan 2011; accepted 30 Jan 2011; published 16 Feb 2011

modeled by a Lorentz oscillator dispersive dielectric function, which can be expressed as followed [32, 33]:

$$\varepsilon_r(E) = \varepsilon_b + \frac{B}{E_0^2 - E^2 + j\Gamma E}, \quad (1)$$

where E_0 is the exciton transition energy. The physical parameter B is related to the exciton oscillator strength and Γ is the broadening parameter.

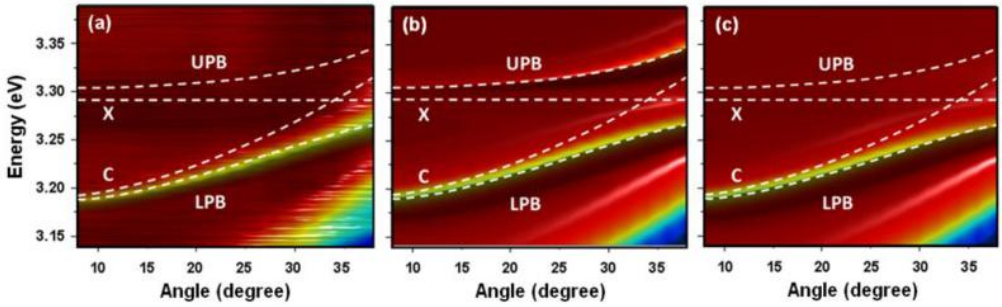

Fig. 3. (a) Color map of the angular dispersion of measured reflectivity spectra from 8 to 38° at RT. The reflectivity spectra are normalized for the purpose of highlighting the variation of polariton dispersion curves. (b) Color maps of the calculated angle-resolved reflectivity spectra with taking into account the resonant exciton. (c) Simulation of angle-resolved reflectivity spectra for the bulk ZnO MCs after considering the absorption of scattering states.

In Fig. 3, the reflectivity spectra are normalized for the purpose of highlighting the variation of polariton dispersion curves and the dashed white lines represent the calculated dispersion curves including exciton mode (*X*), cavity mode (*C*), lower polariton branch (LPB), and upper polariton branch (UPB) by the transfer matrix method. The measured dispersion of the LPB obviously deviates from the parabolic cavity mode and approaches to exciton mode with increasing angle. Furthermore, a good agreement is found between the experimental and theoretical LPBs, as shown in Figs. 3(a) and 3(b), when we consider the strong exciton-photon coupling in our calculation by assigning the parameter related to the oscillator strength of about 10^5 meV^2, which is larger than our previous results and may originate from the probe of the local high quality MCs and the improvement of optical measurement configuration to obtain the more precise experimental results. This value is larger than that of GaN-based materials due to the larger oscillator strength of ZnO materials [32–34,]. As can be seen from Fig. 3(b), we estimated that the anticrossing occurs near the angle of about 34° and the corresponding vacuum Rabi splitting value is about 72 meV. This large vacuum Rabi splitting is larger than recent reports [19–21], which may originate from the high cavity quality factor, good ZnO crystal quality, and larger ZnO thickness. On the other hand, although the angular dispersion of the LPB is well observed from experimental results, the signature of the UPB is nearly not visible.

This interesting issue regarding the anticrossing behavior in bulk ZnO MCs was reported by Faure *et al.* in 2008 [24]. They theoretically expected that the anticrossing behavior can be properly defined in bulk GaAs and GaN MCs, whereas only the LPB is a well-defined and well-mixed exciton-photon state in bulk ZnO MCs. They proposed that the UPB in bulk ZnO MCs is pushed into the continuum states of excitons due to the large vacuum Rabi splitting of 120 meV (i.e., twice larger than the exciton binding energy) in their calculation. Nevertheless, the Rabi splitting estimated in our structure is about 72 meV, which is only slightly larger than the exciton binding energy. Therefore, the UPB will not overlap with the exciton continuum states. To understand the origin of the invisible UPB in the bulk ZnO MC, except for the exciton continuum states, we further take into account the effect of absorption induced by scattering states of excitons in our simulation. The 3D exciton physical model is used in

#138784 - $15.00 USD Received 29 Nov 2010; revised 3 Jan 2011; accepted 30 Jan 2011; published 16 Feb 2011

our calculation to involve the absorption of bound states and continuum states, which can be described as [35].

$$\alpha(\hbar\omega) = \frac{A_0}{2\pi^2 R_y a_0^3}\left[4\sum \frac{\gamma / n^3}{\left(\chi + 1/n^2\right)^2 + \gamma^2} + \int \frac{d\chi'}{\pi} \frac{\gamma S_{3D}(\chi')\sqrt{\chi'}}{\left(\chi - \chi'\right)^2 + \gamma^2}\right], \qquad (2)$$

where R_y is the exciton Rydberg energy, a_0 is the exciton Bohr radius, γ is the half-linewidth normalized by Rydberg, χ is a normalized energy $(\hbar\omega - E_g)/R_y$, and S_{3D} is the Sommerfeld enhancement factor

$$S_{3D}(\chi) = \frac{2\pi / \sqrt{\chi}}{1 - e^{-2\pi/\sqrt{\chi}}}. \qquad (3)$$

The corresponding parameters were extracted from the recent literature [24]. The scattering states can be understood by the combination of various broadening bound states and continuum states. These effects are considered in the broadening terms of the physical model. The absorption due to scattering states is added into the dielectric function and the amplitude is adjusted to match the experimental absorption spectra.

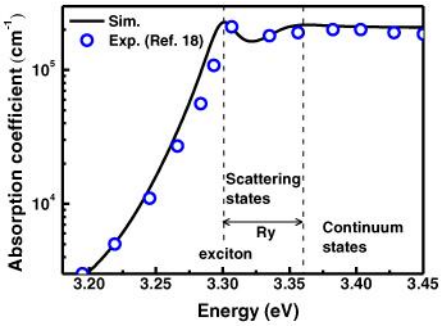

Fig. 4. Experimental (open blue circle) [36] and simulated (solid line) absorption spectra of a bulk ZnO at RT.

Figure 4 shows the experimental (open blue circle) and simulated (solid line) absorption spectra of a bulk ZnO at RT. The experimental spectrum was taken from the result reported by Jellison and Boatner [36]. Although the absorption spectrum of a bulk ZnO is different from that of a ZnO film grown on nitride-based DBRs in the shape of the absorption edge, the absorption coefficients in the spectral range of exciton scattering and continuum states are more significant in this study. For an ideal case, the energy states of an exciton are quantized and the energy states higher than the exciton binding energy are continuum states. Therefore, in the energy range between the exciton ground state and the onset of the continuum states, there should be quantized exciton excited states with sharp absorption peaks. However, scattering states are described in a model going beyond the simple scheme. In this frame, excitons are discrete states and scattering states form a continuum which has neither the density of states nor the absorption of a continuum, and is modeled by Eq. (2) by adding the broadening terms. It may originate from the exciton excited states, the onset of continuum absorption, and the exciton-phonon interaction, especially at RT. In this study, we highlight the difference between continuum and scattering states since the Rabi splitting estimated in our structure is about 72 meV, which is comparable with the exciton binding energy. Therefore, when the vacuum Rabi splitting energy is nearly the same as the exciton binding energy, it will give rise to the energy overlap between the UPB and the scattering states. Figure 3(c) presents the simulation of angle-resolved reflectivity spectra for the bulk ZnO MCs after taking the scattering states and continuum states absorption into account. It is

#138784 - $15.00 USD Received 29 Nov 2010; revised 3 Jan 2011; accepted 30 Jan 2011; published 16 Feb 2011

clearly observed that the UPB is significantly broadened due to its crossing with the scattering states of excitons. Such a situation is especially important for bulk ZnO MCs due to the relatively thick cavity layer and the large absorption coefficient (~2×10^5 cm^{-1}) for ZnO materials [24]. These effects induce the damping of the coherence for upper polariton states and lead to the dispersion of UPB to be invisible. Although the full anticrossing behavior cannot be experimentally demonstrated because of the strong scattering absorption, it should be noted that clear observation of the LPB is more important for the investigation of Bose-Einstein condensation and polariton lasing. Prospects regarding the experimental observation of the complete anticrossing behavior may be achieved based on a ZnO/ZnMgO quantum-well-MC due to the decrease in the thickness of ZnO absorption and the enhancement of exciton binding energies, pushing the continuum states of exciton to higher energy values due to the 2D excitonic nature from the quantum confinement effect.

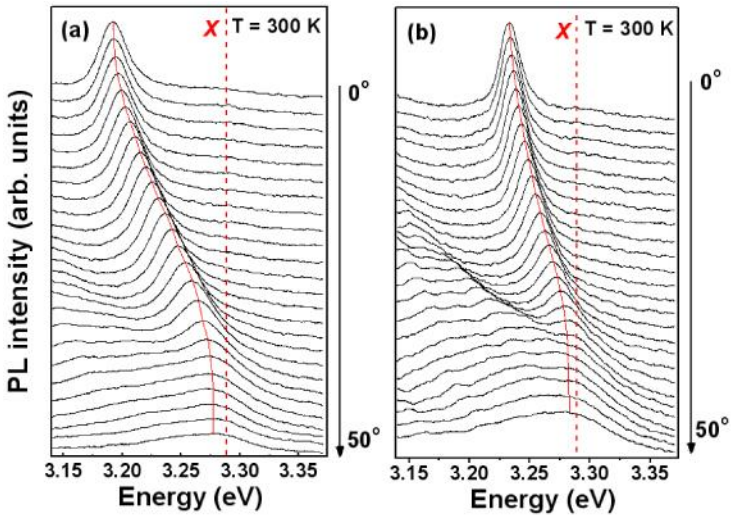

Fig. 5. The experimental angle-resolved PL spectra of the ZnO MCs with approximate exciton-photon detunings of: (a) δ = –78 meV, and (b) δ = –26 meV at RT. The dashed line corresponds to the uncoupled exciton energy. The curve red line is a guide for the eyes, showing the dispersion of lower polariton branch.

3.2 Polariton relaxation bottleneck and its suppression

To further confirm the PL emission originated from the LPB, the sample was studied by angle-resolved PL at RT. Two different detunings between the uncoupled photon and exciton modes at zero in-plane wave vector were considered to confirm the strong coupling phenomenon. Figure 5 presents the experimental angle-resolved PL spectra of the ZnO MCs with approximate detunings of: (a) δ= –78 meV, and (b) δ= –26 meV at RT. The dashed line corresponds to the uncoupled exciton energy. Instead of a pure cavity mode following a parabolic dispersion, the LPB can be observed in these two cases. The photonlike LPB will approach to excitonlike LPB with increasing the measurement angle and finally converges to an energy that is close to uncoupled exciton.

#138784 - $15.00 USD Received 29 Nov 2010; revised 3 Jan 2011; accepted 30 Jan 2011; published 16 Feb 2011

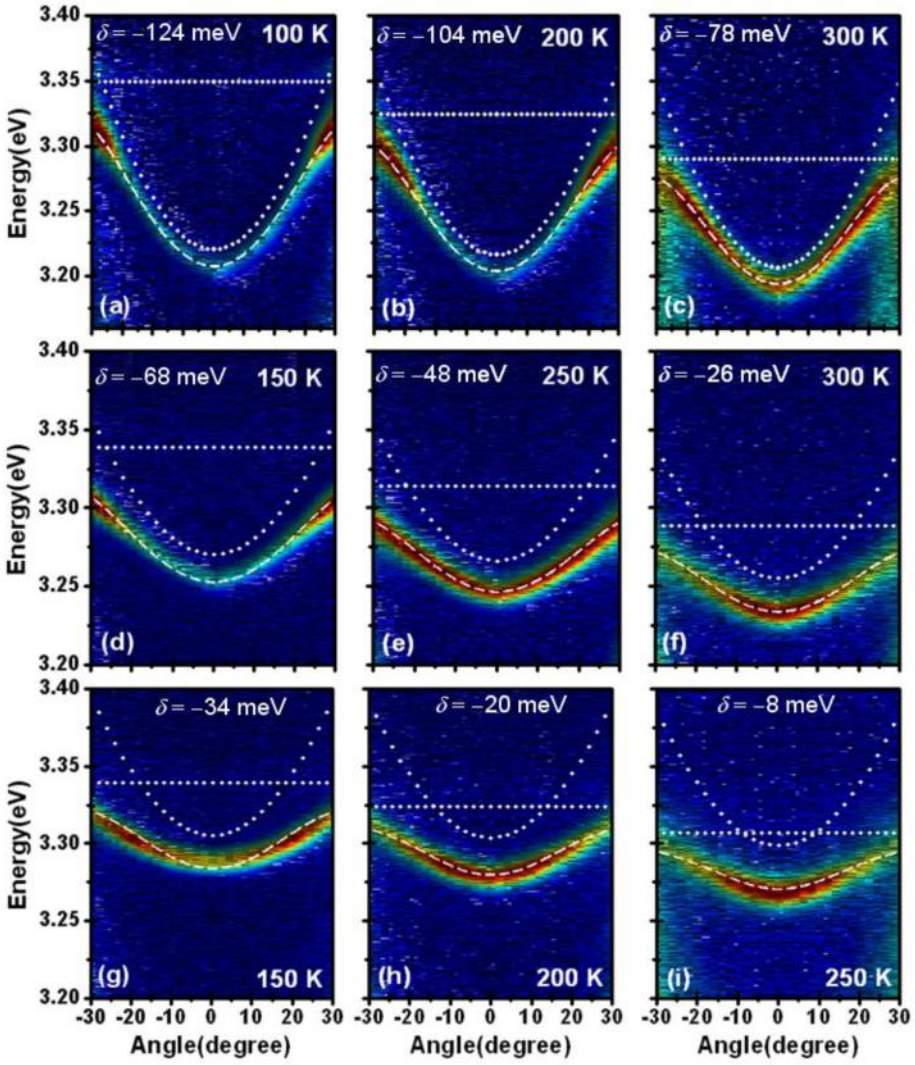

Fig. 6. 2D color map of the PL intensity vs. energy and angle from the sample normal direction for three different positions on the sample with different detuning. The PL intensities are normalized to the maximum for each temperature and detuning. The horizontal dot lines show the exciton energies and the curve dashed and dotted lines represent the coupled LPB and uncoupled cavity photon mode, respectively.

#138784 - $15.00 USD Received 29 Nov 2010; revised 3 Jan 2011; accepted 30 Jan 2011; published 16 Feb 2011

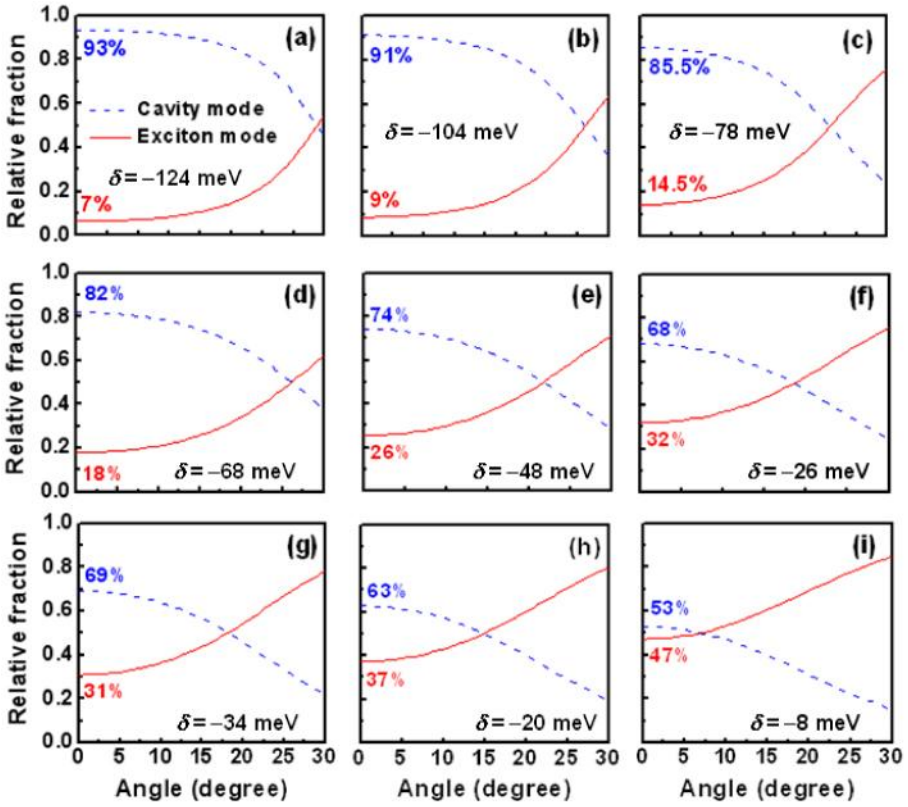

Fig. 7. The calculated exciton and cavity photon fractions for different exciton-photon detunings. There is a one-to-one correspondence between the mappings in Fig. 6 and the each of the calculated fractions vs. angle in Fig. 7 based on the same exciton-photon detunings.

To get a better understanding of the polariton occupancy and the corresponding competition between relaxation and emission processes, we measured the polariton population distribution by time-integrated, angle-resolved PL. Figure 6 shows the 2D color map of the PL intensity vs. energy and angle from the sample normal direction for three different positions on the sample with different detunings at temperature between 100 and 300 K. The PL intensities are normalized to the maximum for each temperature and detuning. The energy of uncoupled excitons from the half-cavity structure was measured by means of PL for different temperatures, as indicated by the horizontal dotted lines in Fig. 6. Using cavity detuning δ and temperature-dependent exciton-photon coupling strength Ω as fitting parameters, the data for the lower polariton dispersions can be fitted by the following relationship:

$$E_{LP}(\theta) = \frac{1}{2}\left[E_C + E_X - \sqrt{\Omega^2 + \delta^2} \right], \tag{4}$$

where the complex energies for the uncoupled exciton E_X and cavity-photon E_C are taken into account. The real part represents the uncoupled exciton or photon energies and the imaginary part represents the broadening related to the lifetime. The broadening of cavity photon modes is considered by using the transfer matrix method to calculate the full MC with DBRs. By applying this model, the fitting parameters are the broadening of exciton and the exciton-photon coupling strength. The fitted LPBs and cavity dispersions are shown by the dashed and dotted lines, respectively. According to the calculated results, the Rabi splitting (around 70 meV) slightly decreases with increasing temperature, which was also observed in recent

#138784 - $15.00 USD Received 29 Nov 2010; revised 3 Jan 2011; accepted 30 Jan 2011; published 16 Feb 2011

studies [21, 23], and may be stemmed from a decrease of the exciton oscillator strength with increasing temperature due to the reduction of the static dielectric constant [23]. On the other hand, the fitting curves shown in Fig. 6 have small deviation as compared with measured results, which may be due to the difficulty in precisely considering all the temperature-dependent parameters, including exciton energies, cavity modes, broadening terms, and oscillator strength. Nevertheless, this small deviation should not influence the trend of the polariton relaxation as a function of temperature and detuning.

Figures 6(a)–6(c) show the results of a MC with the largest negative detuning (δ= −78 meV at RT). Bottleneck persists from 100 up to 300 K. But a strong redistribution of the polariton population is found with increasing temperature. It shows inefficient scattering of bottleneck polaritons into the ground state at large negative detunings. The temperature-dependent detuning δ will also influence the distribution of polariton emission due to the different exciton and photon fractions of the polariton states. The exciton and photon contents in the mixed polariton states are calculated using a 2×2 matrix to obtain the expansion coefficients of the eigenstates on the exciton and photon basis. The results shown in Fig. 7 have one-to-one correspondence between the mappings in Fig. 6 and the each of the calculated fraction vs. angle in Fig. 7 based on the same detunings. The effect of bottleneck suppression is more clearly seen in Figs. 6(d)–6(f), at a smaller detuning (δ= −26 meV at RT). The bottleneck is obvious at 150 K when the photon fraction is about 82%. Uniform emission intensity ranging over 30° exhibits the dynamic competition between the phonon-assisted polariton relaxation and the escape of cavity photons at 250 K, as shown in Fig. 6(e). When the temperature rises to 300 K, the maximum emission intensity is centered at zero degree and a relaxation bottleneck is absent due to the increased polariton-phonon interaction and the lower photon fraction of 68%. Figures 6(g)–6(i) show the results at an even smaller detuning (−8 meV at 250 K). It can be observed that the polariton relaxation bottleneck is effectively suppressed at this smaller detuning even if the temperature is well below RT. Comparing Figs. 6(f) and 6(g), we find that at similar photon fractions ~69% (i.e., at similar detuning), the polaritons can scatter more efficiently from high k states into lower k states by increasing the temperature from 150 to 300 K. Similar situation can also be found between Figs. 6(c) and 6(d). Therefore, at a fixed detuning, the increase of temperature is responsible for the more efficient relaxation of polaritons. On the other hand, given a same temperature of 200 K, polariton bottleneck is also suppressed when the photon fraction is reduced from 91% to 63% [see Figs. 6(b) and 6(h),]. It shows that a flatter dispersion and longer polariton lifetime are sufficient for suppressing the relaxation bottleneck at the relatively lower temperature of 200 K.

In addition to the effect of polariton-phonon interaction, the role of stimulated scattering and polariton-polariton scattering was studied by measuring the pumping power dependence of angled resolved PL at 150 K for the detuning of −26 meV. As shown in Fig. 8, the incident power density is varied from 30 to 90 W/cm^2, corresponding to pulse energy density from 0.6 mJ cm^{-2}/pulse to 1.8 mJ cm^{-2}/pulse. The intensities given in Fig. 8 represent the integrated PL intensity and the peak intensities for different pumping powers were normalized to unity in order to clearly observe the distribution of the polariton emission versus angle at low and high pumping power densities. The PL intensity at small angles increases with excitation and a suppression of the relaxation bottleneck was observed. The polaritons relax from high k states more efficiently through stimulated scattering with increasing pumping power [18].

#138784 - $15.00 USD Received 29 Nov 2010; revised 3 Jan 2011; accepted 30 Jan 2011; published 16 Feb 2011

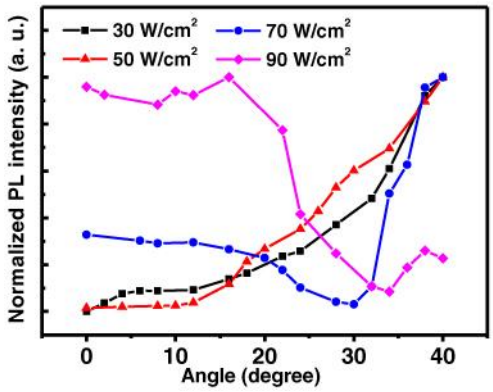

Fig. 8. PL intensities as a function of the detection angle for different excitation power densities at a temperature of 150 K for the detuning of −26 meV.

4. Conclusion

In summary, the strong exciton-photon coupling at RT in bulk ZnO-based hybrid MCs has been demonstrated according to the excellent agreement between experimental and theoretical angle-resolved reflectivity spectra. The large vacuum Rabi splitting of the order of 72 meV is achieved in the ZnO MCs at RT. Furthermore, it is found that the UPB could not be experimentally probed in the thick bulk ZnO MCs since the Rabi splitting energy is larger than the exciton binding energy, pushing the UPB into the energies of scattering states absorption. However, the clear observation of the LPB is a significant step toward the realization of polariton-based optoelectronic devices for ZnO-based semiconductor MCs. Furthermore, the polariton relaxation bottleneck has been observed in bulk ZnO-based MCs by performing angle-resolved PL measurements. The relaxation of the polariton bottleneck towards low k states can be enhanced with increasing temperature and decreasing cavity-exciton detuning. In the case of large exciton-photon detuning δ = −78 meV at RT, the relaxation bottleneck cannot be completely suppressed even if the temperature is increased to 300 K due to the high photon fraction of polaritons at low k states. In the case of small exciton-photon detuning δ = −8 meV at 250 K, the lower photon fraction results in longer polariton lifetime sufficient for the relaxation process into low k states even though the temperature is only 200 K. These results will assist a better understanding of polariton dynamics in ZnO-based MCs, and will provide guidance for designing ZnO-based exciton-polariton experiments and devices.

Acknowledgments

The authors would like to gratefully acknowledge Prof. Yamamoto at Stanford University for his fruitful suggestion. This work has been supported in part by the MOE ATU program and in part by the National Science Council of Republic of China (ROC) in Taiwan under Contract NSC 99-2221-E-009-035-MY3, NSC 99-2120-M-009-007, and NSC 98-2923-E-009-001-MY3.

#138784 - $15.00 USD Received 29 Nov 2010; revised 3 Jan 2011; accepted 30 Jan 2011; published 16 Feb 2011